PLOS ONE

RESEARCH ARTICLE

Ventricular outflow tract obstruction: An *in-silico* model to relate the obstruction to hemodynamic quantities in cardiac paediatric patients

Giulia Comunale[1]*, Massimo Padalino[2], Carmelo Maiorana[3], Giovanni Di Salvo[4], Francesca M. Susin[1]

1 Cardiovascular Fluid Dynamics Laboratory HER, Department of Civil, Environmental and Architectural Engineering–University of Padova, Padova, Italy, **2** Paediatric and Congenital Cardiovascular Surgery Unit, Department of Cardio-thoracic and Vascular Sciences and Public Health, University of Padova Medical School, Padova, Italy, **3** Department of Civil, Environmental and Architectural Engineering–University of Padova, Padova, Italy, **4** Paediatric Cardiology, Department of Woman and Child's Health, University of Padova Medical School, Padova, Italy

* giulia.comunale@dicea.unipd.it

Citation: Comunale G, Padalino M, Maiorana C, Di Salvo G, Susin FM (2021) Ventricular outflow tract obstruction: An *in-silico* model to relate the obstruction to hemodynamic quantities in cardiac paediatric patients. PLoS ONE 16(10): e0258225. https://doi.org/10.1371/journal.pone.0258225

Editor: Lucio Careddu, Policlinico S. Orsola-Malpighi, ITALY

Received: May 12, 2021

Accepted: September 21, 2021

Published: October 15, 2021

Data Availability Statement: All relevant data are within the manuscript and its Supporting Information Files.

Funding: The study was partially supported by the "Ministero dell'istruzione, dell'università e della ricerca" (Award Number PRIN 20177TTP3S_004).

Competing interests: The authors have declared that no competing interests exist.

Abstract

Background

Right (R) or left (L) ventricular outflow tract (VOT) obstruction can be either a dynamic phenomenon or a congenital anatomic lesion, which requires a prompt and optimal timing of treatment to avoid a pathological ventricular remodelling.

Objective

To develop a simple and reliable numerical tool able to relate the R/L obstruction size with the pressure gradient and the cardiac output. To provide indication of the obstruction severity and be of help in the clinical management of patients and designing the surgical treatment for obstruction mitigation.

Methods

Blood flow across the obstruction is described according to the classical theory of one-dimensional flow, with the obstruction uniquely characterized by its size. Hemodynamics of complete circulation is simulated according to the lumped parameter approach. The case of a 2 years-old baby is reproduced, with the occlusion placed in either the R/ or the L/VOT. Conditions from wide open to almost complete obstruction are reproduced.

Results

Both R/LVOT obstruction in the *in-silico* model resulted in an increased pressure gradient and a decreased cardiac output, proportional to the severity of the VOT obstruction and dependent on the R/L location of the obstruction itself, as it is clinically observed.

Conclusion

The *in-silico* model of ventricular obstruction which simulates pressure gradient and/or cardiac output agrees with clinical data, and is a first step towards the creation of a tool that can support the clinical management of patients from diagnosis to surgical treatments.

Introduction

Obstruction of the right (R) or left (L) ventricular outflow tract (VOT) is a common pathological cardiac disease which is characterized by a partial or a complete VOT obstruction that causes several hemodynamic and pathological changes. This pathology may be congenital or acquired, and may cause ventricular dysfunction and symptoms at any age. When congenital, VOT obstruction may be involving the right or left ventricular outflow tract with a spectrum of disorders. For example, in the paediatric population, a right ventricular outflow tract obstruction (RVOTO) may be due to a defect in the pulmonic valve, the supravalvar region, the infundibulum, or the pulmonary artery, and include pulmonary atresia or stenosis, and tetralogy of Fallot [1]. Analogously, a left ventricular outflow tract obstruction (LVOTO) may be due to a defect in the aortic valve, or a defect located at the subvalvar or supravalvar level, and include aortic valve stenosis, coarctation of the aorta and hypoplastic left heart syndrome [2]. Moreover, R/LVOTO may also be caused by primary cardiac tumours in the proximity of the pulmonary or aortic valve. These cardiac tumours arise in the heart, and, usually, they are characterized by round or oval shape with a smooth or lobulated surface [3].

Despite the clinical relevance of VOT obstruction (e.g., aortic valve stenosis alone, which accounts for 3% to 6% of congenital heart disease (CHD), has an incidence of 2.5–6 per 10000 live births [2]), several lacunae still exist.

i) From the clinical point of view, the accurate non-invasive prediction of VOT severity for appropriate timing of intervention is still challenging [4]. The indications for treatment of R/LVOT obstruction, reported by the American Heart Association [5], refer to the peak-to-peak ventriculo-arterial gradient derived by cardiac catheterization in sedated patients. This value is consistently lower than what obtained by echocardiography, which is the most common measurement used to assess disease severity in clinical practice [2]. This is particularly significant in those patients with small aortic or pulmonary arterial diameters, e.g., paediatric population [4, 6]. Moreover, notice also that how the obstruction geometry affects the pressure gradient is one further open question [4]. For these reasons, the obstruction evaluation by echocardiography may be unsuitable due to overestimation of the pressure gradient, resulting in misclassification of the disease severity and leading to inappropriate timing of intervention.

ii) To the best of our knowledge, currently engineering research has focused its attention almost exclusively to aortic valve stenosis [7–9]. The physical and mathematical-numerical models that have been proposed over the years to describe aortic transvalvular hemodynamics are numerous, and with varying degrees of detail e.g., from bulk flow parameters to local flow kinematic and dynamics, from rigid valve geometry to time dependent geometry, calcification modelling, and so on [8–12]. Modelling of obstructive diseases other than aortic stenosis has been only sporadic and limited to the adult population. Thus, developing a mathematical model that can relate the percentage of VOT diameter reduction (i.e., obstruction) to the pressure gradient and the cardiac output may help to overcome the stated drawbacks with the final goal to optimize diagnosis of an obstructive disease, and clinical management.

In this study, we aimed to derive a numerical model that can reproduce the hemodynamic changes occurring with R/LVOT obstruction, and to relate the percentage of restriction to

overall hemodynamic quantities. A lumped-parameter model of the complete circulation is hence coupled to a local model of hemodynamics through the narrowing, being fixed the degree of obstruction. As a result, the model gives both the cardiac output and the pressure gradient through the narrow tract. We applied the model to a paediatric case since VOT obstruction in infants may become hemodynamically significant earlier than in adults, due to the rapid rate of growth and the small cardiac dimensions [13], and echocardiographic assessment may be misled. Nevertheless, note that the model can be easily adapted to the adult case by appropriately tuning the model's parameters.

Methods

In-silico model

From the fluid dynamic point of view any cardiovascular obstruction, located in either vessels or heart chambers, can be seen as an obstacle to blood flow and, as such, as a source of disturbances that subtract mechanical energy to the bulk flow in the form of an irreversible pressure loss. When the bulk flow develops along one main direction, as in the case of vessels or, for the heart chambers, in the left or right ventricular outflow tract, seen as a cylindrical conduit [14, 15], the behaviour of the obstructed blood flow can be effectively described by means of the classical equations of one-dimensional hydrodynamics [16]. Such an approach, which allows for the evaluation of global hemodynamic parameters, has been widely adopted to investigate cardiovascular flows in either physiological or pathological conditions. For example, a large amount of work has been done in the past twenty years to develop mathematical models able to reliably predict the pressure gradient across a stenotic aortic valve [7, 9].

Here, following that same approach, the blood flow through an obstruction located in either R/LVOT (such as a localized tumour mass, a subvalvular stenosis, or a supravalvular stenosis) is assimilated to the one-dimensional flow in a circular pipe of diameter D and area A, partly occluded by the obstruction (Fig 1A). The latter is geometrically described by the minimum cross-sectional area that the obstacle locally leaves free to the bulk flow, A_{free}, and is considered of negligible length [14]. Due to the narrowing of the pipe, the flow is not able to maintain its proximal undisturbed character but rather behaves as depicted in Fig 1B i.e., it initially contracts up to the minimum area and then expands exhibiting distal vortices that cause irreversible viscous energy dissipation. As a consequence, blood velocity increases (decreases) due to the flow area contraction (expansion) and blood pressure does the opposite. However, viscous losses impede the pressure to fully recover so that the pressure gradient Δp_{obs} between the left (right) ventricle and the section distal to the obstruction develops. The gradient can hence be calculated as (see S1 File for details)

$$\Delta p_{obs} = K_{obs} \cdot Q^2 \tag{1}$$

where Q is the (instantaneous) flow rate through the obstruction (i.e., the flow rate ejected by the left or the right ventricle, depending on the obstruction location) and K_{obs} is a coefficient that depends on the shape and size of the obstacle. Following the approach reported in [7], the latter is here assumed as

$$K_{obs} = f_{shape} \frac{\rho}{2} \left(\frac{1}{A_{free}} - \frac{1}{A} \right)^2 \tag{2}$$

with ρ the blood density and f_{shape} a factor ≥ 1 that accounts for the obstruction morphology. Notice that $f_{shape} = 1$ corresponds to the case of an ideal round, annular, concentric obstacle (Fig 2). Notice also that Eq (2) assumes negligible friction losses along the stenotic lesion i.e., a

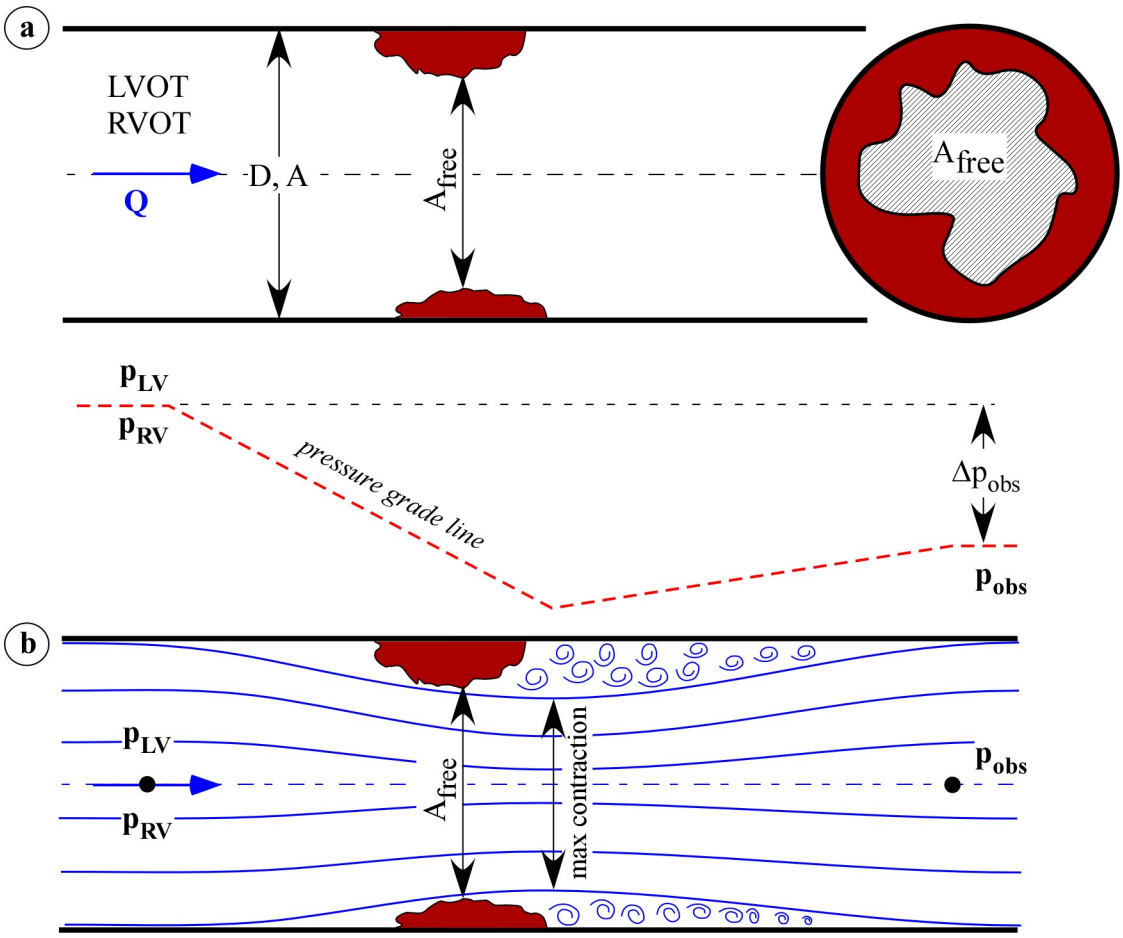

Fig 1. (a) Scheme of the ventricular outflow tract simulated as a one-dimensional flow in a circular pipe of diameter D and area A. The obstruction reduces the cross-sectional area to the minimum A_{free}. (b) Streamlines of the flow and the pressure grade line (red dotted line) due to the presence of the obstruction. The obstruction causes a pressure drop which is only partially recovered in the downstream section, determining a pressure gradient Δp_{obs}. Eddies are present only on the downward section toward the artery. Q, the flow rate, p_{LV} (p_{RV}), pressure in the left (right) ventricle, and p_{obs}, pressure distal to the obstruction.

https://doi.org/10.1371/journal.pone.0258225.g001

localized constriction mainly subjected to mechanical energy losses due to wall separation phenomena is considered [14].

Eqs (1) and (2) represent the mathematical model of the flow in the narrowing, and allow the calculation of the pressure gradient across the obstruction Δp_{obs} given the narrowing ratio

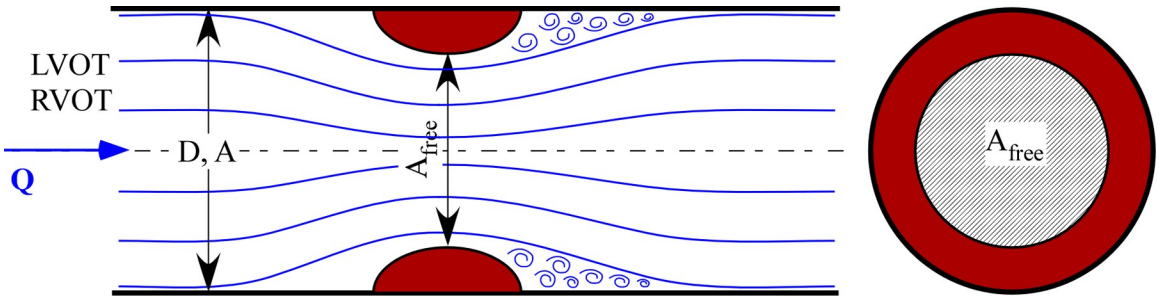

Fig 2. Streamlines of the flow due to the presence of an ideal round obstruction.

https://doi.org/10.1371/journal.pone.0258225.g002

A_{free}/A and the ejected flow rate Q. However, it is worth stressing that the presence of the obstruction in the R/LVOT may induce progressive ventricular dysfunction due to prolonged increased afterload, and ultimately reduce ventricular stroke volume and hence the flow rate Q and the cardiac output, CO. For that reason, and in order to compute not only Δp_{obs} but also Q and CO as a function of A_{free}/A, Eqs (1) and (2) are coupled to a previously developed lumped parameter model (0D) of the complete cardiovascular circulation [17]. The 0D model reduces the cardiovascular system to the sum of multiple functional compartments (e.g., atria and ventricles, large vessels, microvasculature), and describes the hydrodynamic functionality of each compartment by suitably relating the local instantaneous pressure and blood flow rate/volume. Parameters peculiar to each compartment (e.g., heart chambers' elastance, large vessels' compliance, microvasculature's resistance) are adopted to characterize the compartment functionality and account for its effect on the complete circulation. As a result, the instantaneous pressure and flow rate are obtained in each compartment from the 0D model. A complete description of the model itself is given in S3 File. Here, we just recall that the model describes the flow across the heart valves by a relationship of the kind $\Delta p_v = R_v \cdot Q$, where Δp_v is the transvalvular pressure drop and R_v is the valve resistance parameter. For the aortic and pulmonary valve case, in particular, values for R_v are assumed such that normo-functioning valves are simulated i.e., the pressure gradient across the valve results to be negligible (mean value of Δp_v around 1–2 mmHg) and does not affect the pressure gradient due to the obstruction located in the ventricular outflow tract.

Simulations

Conditions pertaining to preserved cardiovascular functionality were reproduced despite the presence of the obstruction i.e., no compensatory mechanism was accounted for even in the most severe obstruction condition. A child case of about 2-years-old with a heart rate HR = 105 bpm, body surface area BSA = 0.55 m^2, body mass BM = 12 Kg, and left (right) ventricular outflow tract diameter D = 0.9 cm (D = 1.07 cm) was considered [18]. Physiological values for that case were assigned to the functional parameters contained in the 0D model (see S4 File).

The 0D model alone was first implemented (i.e., no obstruction in either the left or the right ventricular outflow tract was considered) to compute healthy hemodynamics and compare results with clinical data for model validation. Then, the 0D model coupled with Eq (1) and (2) was repeatedly run to reproduce the cardiovascular circulation in presence of the obstruction. Both the cases of obstruction located in the left and in the right ventricular outflow tract were investigated. Simulations were performed for various degrees of obstruction severity by varying the narrowing ratio A_{free}/A in the range 0.05–1, 1 being the case of VOT free from obstruction and 0.05 the case of VOT almost completely occluded. Lower A_{free}/A ratios were not considered because a further reduction of the flow area determines non-realistic pathological conditions (~ null cardiac output). The shape factor f_{shape} contained in Eq (2) was assumed equal to 1.

Results computed for each obstructed condition were also post-processed to obtain relevant hemodynamic parameters according to the following relationships

$$CO = \frac{1}{T}\int_T Q dt \tag{3}$$

T being the period of one heartbeat;

$$\Delta p_{obs,mean} = \frac{1}{T_e}\int_{T_e} \Delta p_{obs} dt \tag{4}$$

where $\Delta p_{obs,mean}$ is the mean pressure gradient across the obstacle, calculated in the ejection period T_e. The peak value of the gradient, $\Delta p_{obs,peak}$, was extracted as the maximum gradient calculated in one heartbeat.

It has now to be noticed that the pressure gradient routinely estimated by Doppler echocardiography in the clinical non-invasive assessment of a stenotic lesion is not Δp_{obs}. Rather, it is the gradient that establishes between the ventricle and the location of the minimum flow area due to flow acceleration only [9]. The clinical gradient $\Delta p_{Doppler}$ hence does not include the pressure recovery (PR) effect which partially restores the pressure distal to the obstruction [4, 6] and, as a consequence, it is typically larger than Δp_{obs}. In order to compare Δp_{obs} and $\Delta p_{Doppler}$, we hence computed also the latter, by applying the relationship adopted in the clinical practice i.e., the so-called simplified Bernoulli equation

$$\Delta p_{Doppler} = 4 \cdot V_{A_{free}}^2 \tag{5}$$

where $V_{A_{free}}$ is the velocity in the section of minimum flow area, $V_{A_{free}} = Q/A_{free}$. The mean and the peak values of $\Delta p_{Doppler}$ were finally obtained as they were for Δp_{obs}.

A sensitivity analysis of model results to the shape factor f_{shape} was performed, which was varied in a realistic range estimated as explained in S2 File.

Finally, a sensitivity analysis to verify the influence of parameters on the model was carried out and reported in S5 File.

The model was run harnessing the built-in MATLAB® function *ode15s*, solving a closed-loop system. The results were obtained after reaching the periodic steady state and they were validated considering literature data.

Results and discussion

In the clinical setting, a RVOT or LVOT obstruction is a common either congenital or acquired problem. Its clinical management may be compromised by the adoption of the simplified Bernoulli equation used for echocardiography, which does not account for the pressure recovery effect [4, 6]. Beyond that, engineering research has focused almost exclusively on aortic stenosis [7–9], neglecting the wide spectrum of diseases that may cause VOT obstruction. Thus, we developed a mathematical model to correlate the degree of R/LVOT obstruction to the Δp and the cardiac output. The obstructed flow model is very simple, mainly because the lack of detailed clinical data relating the size/morphology of the obstruction and the hemodynamic parameters, in particular in the paediatric population, would make premature any more refined representation. However, real obstructions similar to the simplified one here adopted are not unusual, as for the case of tumour masses in children [3]. Also the lumped model built up for the entire circulation is quite simple, so that parameters can be adequately calibrated also for those patients' cohorts less represented in the literature i.e., when the 'reference patient' is not the average adult male.

Simulations of the healthy condition performed to validate the model compare favourably with literature data, proving a good representation of the reproduced paediatric population: Table 1 reports a quantitative comparison between the output of the healthy child 0D model and literature data for the paediatric population [18]. As it can be seen, global hemodynamic parameters fall within physiological ranges for both the left and right circulation, with differences within the measurement error.

Figs 3 and 4 show the agreement between the computed pressure and flow rate and those given in literature for both the systemic and pulmonary circulation. In particular, Fig 3 shows the physiological aortic pressure and flow rate calculated by the 0D model together with published *in vivo* measurements obtained in paediatric subjects [19, 20]. There is a good

Table 1. Comparison of model outputs with literature data specific for the paediatric case given as physiological ranges [18].

Parameters	Unit	Model Output	Reference
SVR	mmHg*s/mL	2.0	1.5–2.1
SBP	mmHg	93	90–110
DBP	mmHg	64	65–75
p_{RV}	mmHg	18/2**	15-23/3-7
p_{PuA}	mmHg	17/9**	15-23/10-16
p_{LA}	mmHg	5.7*	5–10
p_{LV}	mmHg	94/3**	90-110/7-9
p_{RA}/CVP	mmHg	3.9*	2–6
CO	L/min	2.2	1.3–2.7

HR, heart rate, SVR, systemic vascular resistance, SBP, systolic blood pressure, DBP, diastolic blood pressure, p_{RA}, right atrial pressure, p_{RV}, right ventricular pressure, p_{PuA}, pulmonary artery pressure, p_{LA}, left atrial pressure, p_{LV}, left ventricular pressure, CVP, central venous pressure, CO, cardiac output.

* mean value

** systolic/diastolic values.

https://doi.org/10.1371/journal.pone.0258225.t001

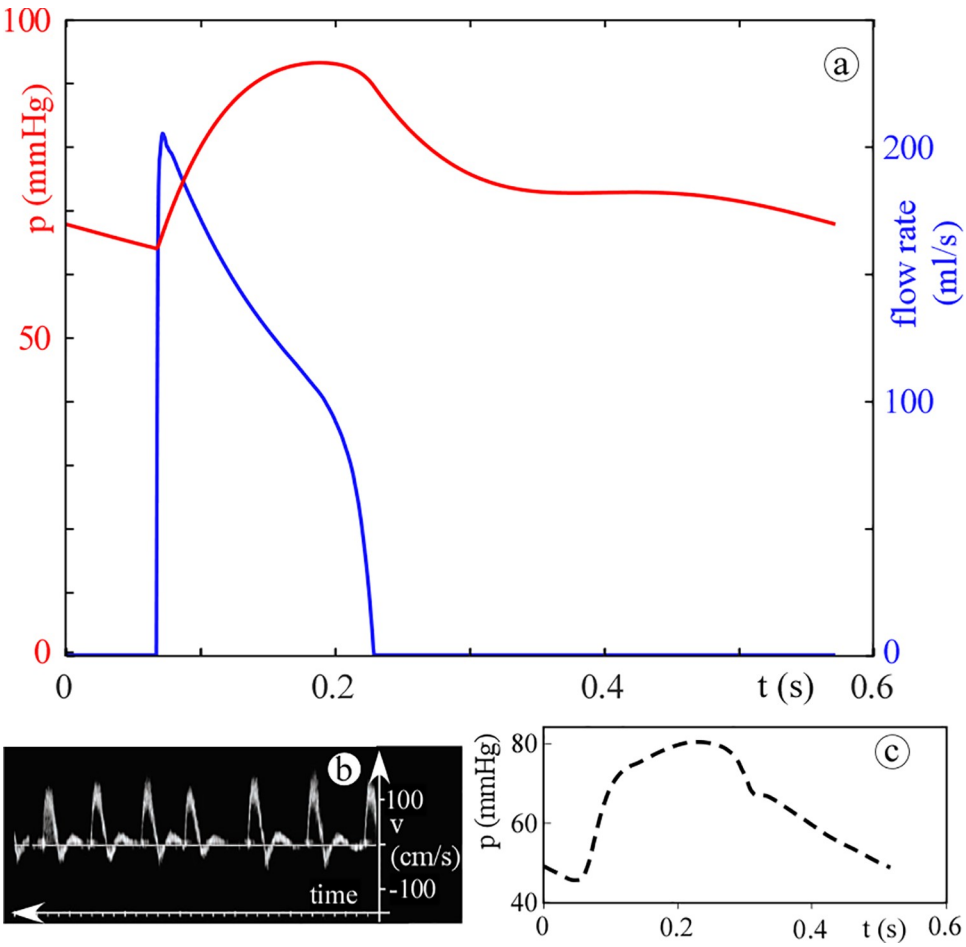

Fig 3. Panel (a): 0D model results for the physiologic case (aortic pressure, red curve; aortic flow rate, blue curve). Panels (b) and (c): published *in-vivo* data (aortic Doppler velocity waveform [19] and aortic pressure [20]). Note that, by assuming a constant valve area, the velocity waveform resembles the flow one except for the absolute values and the scale.

https://doi.org/10.1371/journal.pone.0258225.g003

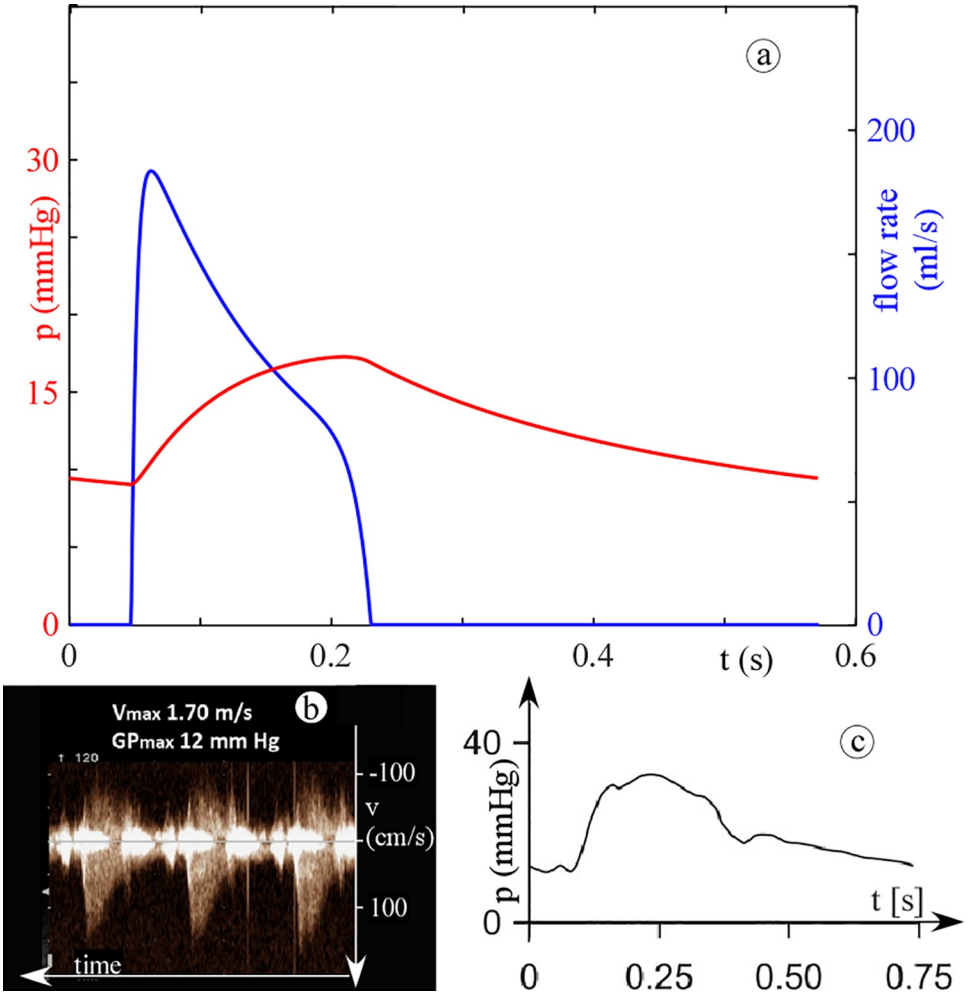

Fig 4. Panel (a): 0D model results for the physiologic case (pulmonary arterial pressure, red curve; pulmonary flow rate, blue curve). Panels (b): [22] and (c): [23] published data (pulmonary Doppler velocity waveform and pulmonary arterial pressure, respectively). Note that, by assuming a constant valve area, the velocity waveform resembles the flow one except for the absolute values and the scale.

https://doi.org/10.1371/journal.pone.0258225.g004

agreement in terms of waveform shapes, and the computed and *in vivo* mean aortic pressure are about 70 and 60 mmHg, respectively. Additionally, from the peak flow rate and velocity of 200 mL/s (Fig 3A) and 150 cm/s (Fig 3B), respectively, an aortic diameter of about 1.3 cm is found. This value agrees with the *in vivo* measurement of Hegde *et al.* [21] for a child with a BSA of 0.55 m^2. Similarly, Fig 4 shows the physiological waveforms for the pulmonary circulation compared to reference data [22, 23]. Note that, for the pulmonary circulation, the references are not age specific. However, the computed waveforms well resemble the physiological characteristics. Notice also that the valve backflow is not computed by the model since only the forward flow is considered (on/off diodes). This simplification does not affect the results since we focused on the ventricular obstructions severity i.e., in the ejection phase only.

Fig 5 compares the results obtained from the model for the physiologic case (panel (a)) and, as an example of obstruction in the LVOT, for the $A_{free}/A = 0.525$ case (panel (b)). As it is evident in Fig 5B, when the obstruction is included in the model at any level in the LV, the LV pressure increases, maintaining the aortic pressure unchanged and resulting in a pressure

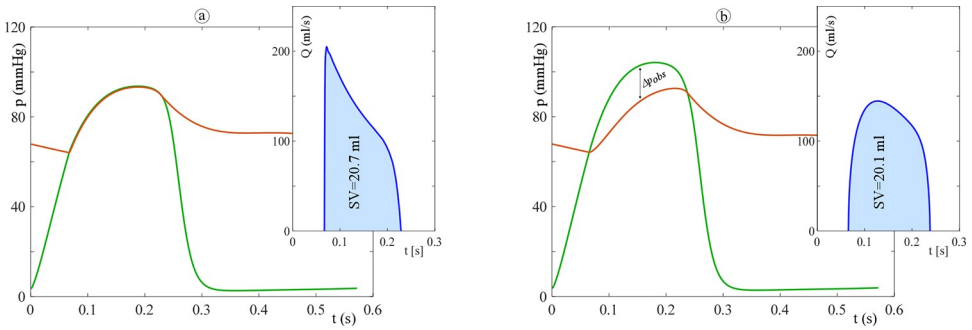

Fig 5. Left ventricle pressure (green), aortic pressure (red), and aortic flow rate (blue) as calculated by the model for the physiologic case (panel (a)) and the case of obstruction located in the LVOT with $A_{free}/A = 0.525$ (panel (b)).

https://doi.org/10.1371/journal.pone.0258225.g005

gradient (Fig 5A). Similar findings are reported by De Vecchi *et al.* [24] for the case of LVOTO after transcatheter mitral valve replacement in adults.

Differently, RVOT obstruction does alter the shape of the pulmonary arterial pressure with the stenotic case exhibiting the typical delayed, lowered, and triangular appearance as stated by Butera *et al.* [25] (see Fig 6). For what the valve flow is concerned, the presence of the obstruction (either in LVOT or in RVOT) also significantly affects the shape of the ejected flow rate

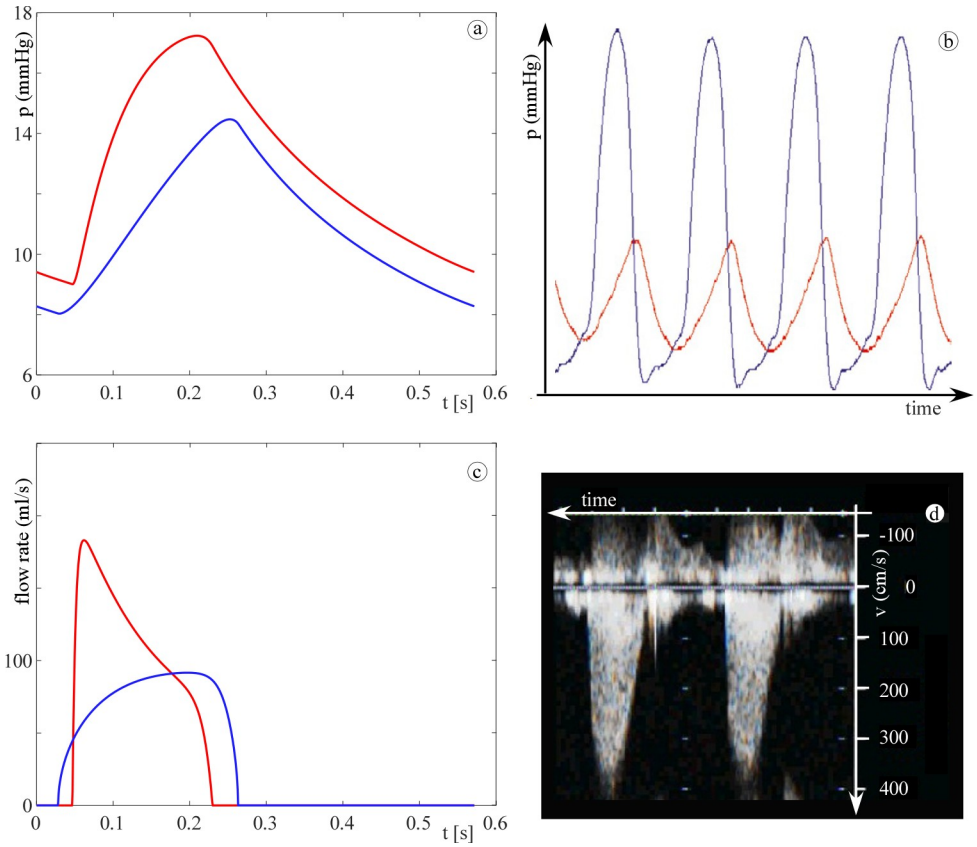

Fig 6. Pulmonary arterial pressure and flow rate. (a) computed pulmonary arterial pressure, (b) stenotic reference data (blue and red, right ventricular and pulmonary arterial pressure, respectively) [25], (c) computed pulmonary flow rate, and (d) stenotic reference data [22]. For the computed waveforms: in red, the healthy condition, and in blue, the stenotic case.

https://doi.org/10.1371/journal.pone.0258225.g006

waveform (Figs 5 and 6). The steepness of the acceleration branch smooths, the branch peaks at a lower flow rate, the time of peak is delayed in the ejection period, which has a longer duration, and, as a result, the waveform moves from a rather triangular to a bell shape. It is worth noting that such a behaviour is recognized to occur in presence of aortic and pulmonary valve stenosis [26–30], which further confirms the robustness of the model in computing obstructed flows characteristics.

Fig 7 shows the behaviour of the mean and the peak pressure gradient across the obstruction as a function of the narrowing ratio A_{free}/A (left panel: LVOT obstructions; right panel: RVOT obstructions). Possible threshold values for the mean (peak) pressure gradient as inferred from the literature for the case of a tumoral obstructive condition are also drawn for comparison [31–33]. As expected, both the mean and the peak pressure gradients, $\Delta p_{obs,mean}$ and $\Delta p_{obs,peak}$, increase as the obstruction becomes more severe. Obstructions located in the LVOT or in the RVOT result in similar exponential behaviour, but a larger rate of change of the gradient with A_{free}/A diminishing is found for left obstructions i.e., LVOT obstructions seem to impact the heart pressure state more heavily than RVOT ones. This behaviour might be related to the recognized capability of the RV to adapt to pulmonary valve stenosis i.e., pressure overload conditions [34].

Results shown in Fig 7 can be of help in estimating the degree of obstruction severity by comparing model computed gradients to threshold values measured in clinical practice. When the R/LVOT obstruction is caused by a mass (i.e., cardiac tumour), reference values for the limit between moderate and severe obstruction can be inferred from the recent literature. Dyspnoeic children with left mean pressure gradient greater than 30 mmHg are reported by Walter *et al.* [32]; the case of a patient with left obstruction reported as moderate, mean gradient 35 mmHg and peak gradient 60 mmHg is described in [31]; finally, Padalino *et al.* [33] define as significant a left or right obstruction with peak gradient larger than 50 mmHg. The comparison of the simulation's outputs with the above clinical thresholds (Fig 7) highlights that moderate/severe obstruction is found for $A_{free}/A \approx 0.3$–0.38 and $A_{free}/A \approx 0.1$–0.15 for LVOT and RVOT obstruction, respectively. Our results show that the computed right critical narrowing ratio might seem so small to be unrealistic. However, this is in agreement with what reported in the clinical field by Foschi *et al.* [34] who stated that "*In moderate-to-severe pulmonary valve stenosis*, *patients remain asymptomatic until adulthood*". Furthermore, the relationships

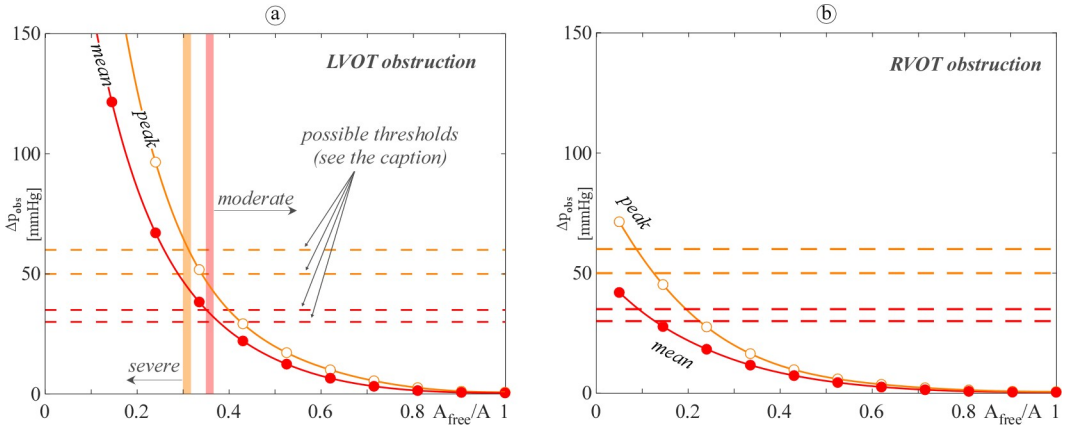

Fig 7. Computed mean (red filled dotted line) and peak (orange open dotted line) pressure gradient for (a) LVOT and (b) RVOT. Dashed lines depict possible thresholds for moderate/severe obstruction, inferred from the literature for the case of a tumoral obstructive condition as it follows: mean gradient 30 mmHg [32] and 35 mmHg [31], red lines; peak gradient 50 mmHg [33] and 60 mmHg [31], orange lines.

https://doi.org/10.1371/journal.pone.0258225.g007

obtained between the gradient and the level of the obstruction may also provide the surgeon with advice in regards to the degree of myocardial resection that she/he should perform to significantly reduce the pressure gradient. For instance, in the LVOT obstruction case, a resection leading to A_{free}/A of about 0.45 is required to diminish the mean pressure gradient below 20 mmHg, which is typically considered the gold standard. Hence, the proposed model is a first step towards a tool that can potentially help in the clinical management of patients. Indeed, there are only few engineering works focused on models for obstructive diseases, especially for studying VOT obstruction of the right ventricle in paediatric patients, which has a high incidence, but is less studied. Thus, models that help in extending knowledge of these pathologies can help in improving both diagnosis and treatment. Indications of the percentage of obstructions can help in identifying the severity of the pathology, and in case of obstructive masses, a suggestion of the amount of mass to be resected can be derived.

When focusing the attention on the obstruction's effects on the cardiac output (Fig 8), it turns out that, RVOT obstructions affect the CO more than what LVOT ones do. In particular, CO = 2.0 L/min (i.e., almost normal) and CO = 0.9 L/min (i.e., significantly depressed) is found when the critical pressure gradient (mean gradient about 30–35 mmHg) is attained in the left and in the right outflow tract, respectively. The model hence captures the recognized lower efficiency of the right ventricle to suitably respond to increased afterload [35, 36], suggesting that critical conditions should be defined in terms of cardiac output rather than of pressure gradient when it is the right outflow tract to be obstructed.

Finally, we further harnessed the model to point out the pressure recovery effect on the evaluation of VOT obstruction, i.e., we compared Δp_{obs} and $\Delta p_{Doppler}$ (Fig 9). We recall that the two above gradients do/do not take into account the pressure recovery, respectively, and that $\Delta p_{Doppler}$ is the gradient clinically evaluated by Doppler echocardiography. As expected in a

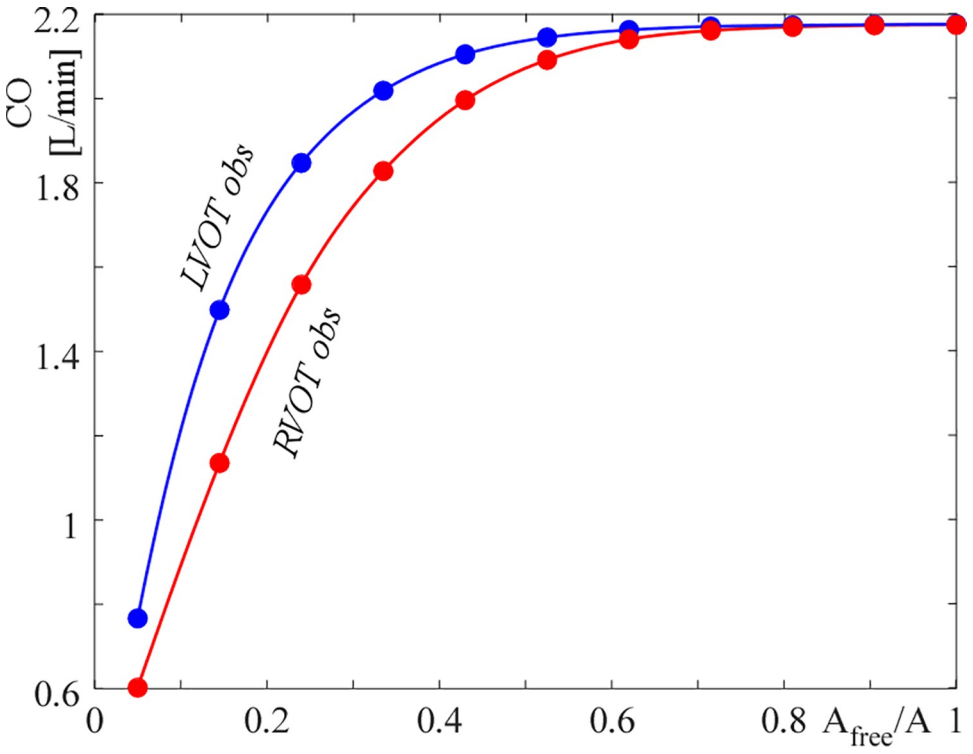

Fig 8. Cardiac output (CO) reduction as the obstruction worsens for LVOT (blue) and RVOT (red) obstructions.

https://doi.org/10.1371/journal.pone.0258225.g008

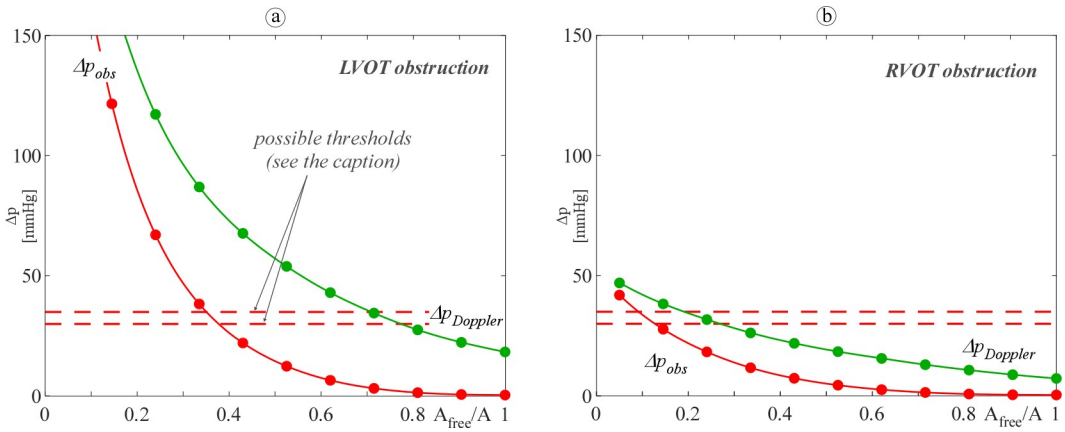

Fig 9. Computed mean pressure gradient with (red filled dotted line, Δp_{obs}) and without (green filled dotted line, $\Delta p_{Doppler}$) the pressure recovery effect for (a) LVOT and (b) RVOT. Red dashed lines depict possible mean gradient thresholds for moderate/severe obstruction, inferred from the literature for the case of a tumoral obstructive condition as it follows: 30 mmHg [32] and 35 mmHg [31].

https://doi.org/10.1371/journal.pone.0258225.g009

paediatric patient, the mean $\Delta p_{Doppler}$ (i.e., the 'pre-recovery' gradient) is larger than the mean Δp_{obs} (i.e., the 'post-recovery' gradient) for both LVOT and RVOT obstruction, and the largest difference falls around moderate obstructions [37] i.e., where the accuracy of the clinical evaluation of the lesion severity is pivotal for the patient management. However, the discrepancy between the two gradients is found to be much more pronounced for LVOT rather than RVOT obstruction. In particular, for the LVOTO case the Doppler gradient overpasses the possible moderate/severe thresholds for values of A_{free}/A even double than those found for Δp_{obs} (A_{free}/A around 0.7 vs A_{free}/A around 0.35, respectively). On the contrary, for the RVOTO case both the computed gradients remain under the thresholds up to A_{free}/A 0.2–0.3. Such a result suggests that not only the pressure recovery affects right lesions much less than the left ones but also that misclassification of lesion severity by Doppler is more likely to occur when the occlusion is located in the left rather than in the right side of the heart. Thus, tools as the one here proposed, which is capable of taking into account the pressure recovery effect, might be of particular help in sparing cardiac catheterization, i.e., invasive procedures, to left side diseased patients.

Limitations and future developments

The adopted shape of the obstruction, described as an ideal round, annular, and concentric narrowing, is the main limitation of our study. Actually, real obstructions might present an irregular geometrical structure, hence our assumption might underestimate the actual value of the loss coefficient K_{obs} in Eq (2). However, a sensitivity analysis of model results to the factor f_{shape} was performed to highlight the relevance of obstacle's shape effects. Calculations show that accounting for a larger contraction of the proximal flow due to the real shape of the obstruction i.e., a larger k_{obs} for the given A_{free}/A, leads to moderate variations of model's outputs for the left case: the critical obstruction (mean and peak Δp_{obs} equal to about 35 and 50 mmHg, respectively) shifts to $A_{free}/A = 0.48$, with cardiac output still around 2.0 L/min. For the right case, the effects of f_{shape} are found to be so small to be undiscernible.

It is also worth noticing that, differently from our assumption, both the right and left VOT shape has been recognized to be more elliptical than circular [38–41]. Our assumption might hence lead to some mis-estimation of stenotic areas. Moreover, VOT geometry might not be

constant during the ejection phase; however, to the best of our knowledge, such a behaviour is not sufficiently described by clinical data to be adequately modelled yet.

The absence of adaptive and remodelling processes which take place in physiological conditions is another limitation of our work. For example, an increase in systemic vascular resistance may counterbalance the effects of the reduced stroke volume and aortic pulse pressure in the case of LVOT obstructions. These aspects will be included in more detail in future work.

Moreover, to further corroborate the model here presented, acquisition and analysis of *in vivo* morpho-hemodynamic data of the obstructed outflow tract, together with obstruction classification based on clinical examination of patients, is strongly recommended. Future work will hence also focus on the creation of a database listing imaging, echo, catheter and other data, and on the comparison of *in vivo* data to model's outputs to optimize the estimation of f_{shape} and K_{obs} for a given size, shape, and type of R/L VOTO.

Finally, it is worth noting that the model has been here applied to a reference paediatric case, but it can be adopted also to reproduce different populations/subgroups/specific patients by properly calibrating hemodynamic parameters. Similarly, by considering sex-specific parameters, sex-related characteristics can be accounted for [17]. For what subgroups examination is concerned, the model can help in investigating the effects of the wide inter-subject variability of the anatomy and pathophysiology. In order to give a preliminary insight in that direction, we run the model for a 10 years-old reference child. Results have shown that both the pressures and the CO are less affected in older than in younger patients by a given A_{free}/A, thus suggesting that older patients better sustain VOT obstructions, in agreement with Singh [42]. It can be speculated that such a result depends on the lower vascular resistances of older patients [18]. Patient-specific simulations are also one of our future goals. For this purpose, non-invasive techniques will be used (e.g., imaging, echo, MR) to evaluate the patient-specific morphology and hemodynamics from which patient-specific parameters will be derived.

Conclusions

Obstruction of the R/L ventricular outflow tract is a common disease, in particular in the paediatric population. Clinical decision-making in the management of patients remains controversial in a significant number of cases. Nonetheless, engineering researches devoted to model ventricular outflow tract obstructive disease are still limited. For this reason, we developed a simple lumped parameter model of hemodynamics in presence of a R/LVOT obstruction, able to give indications on the most significant waveforms, pressure gradient, and cardiac output alterations produced by a given obstruction size.

The lack of clinical data did not allow detailed comparative analysis with physiological measurements of obstructed flows, but model results proved in very good agreement with trends observed in clinical setting thus corroborating the idea that the proposed approach is useful to understand the clinical deterioration of patients and can contribute, with further validation, to the creation of a tool applicable in the clinical practice.

Indeed, the simulations highlighted that the left and right circulations give significantly different response to VOT obstructions. In particular, model predictions suggested that, for the case of right VOTO, the clinical assessment should mainly focus on the CO reduction rather than on the ventriculo-arterial pressure gradient increase. Moreover, the capability of the model of taking into account the pressure recovery effect showed that the model has the potential to become a tool alternative to catheterization, thus preserving borderline patients from invasive procedures. Finally, the design of surgical treatments for obstruction mitigation can benefit from model indications of VOT free area to be restored to accomplish an acceptable pressure gradient/cardiac output.

Supporting information

S1 File. Model of obstructed flow.
(DOCX)

S2 File. Sensitivity analysis of model results to the shape factor f_{shape}.
(DOCX)

S3 File. Model of the complete circulation.
(DOCX)

S4 File. Parameters' values.
(DOCX)

S5 File. Global sensitivity analysis.
(DOCX)

Acknowledgments

The work was developed under the frame of the Infrastructure of Research of the University of Padova INCAS.

Author Contributions

Conceptualization: Giulia Comunale, Massimo Padalino, Carmelo Maiorana, Francesca M. Susin.

Data curation: Giulia Comunale, Francesca M. Susin.

Formal analysis: Giulia Comunale, Massimo Padalino, Giovanni Di Salvo, Francesca M. Susin.

Funding acquisition: Carmelo Maiorana.

Investigation: Giulia Comunale, Francesca M. Susin.

Methodology: Giulia Comunale, Giovanni Di Salvo, Francesca M. Susin.

Software: Giulia Comunale, Francesca M. Susin.

Supervision: Francesca M. Susin.

Validation: Giulia Comunale, Giovanni Di Salvo, Francesca M. Susin.

Visualization: Giulia Comunale, Giovanni Di Salvo, Francesca M. Susin.

Writing – original draft: Giulia Comunale, Francesca M. Susin.

Writing – review & editing: Massimo Padalino, Giovanni Di Salvo, Francesca M. Susin.

References

1. Bashore TM. Adult congenital heart disease: Right ventricular outflow tract lesions. Circulation. 2007; 115: 1933–1947. https://doi.org/10.1161/CIRCULATIONAHA.105.592345 PMID: 17420363
2. Franchi E, Cantinotti M, Assanta N, Viacava C, Arcieri L, Santoro G. State of the art and prospective for percutaneous treatment for left ventricular outflow tract obstruction. Prog Pediatr Cardiol. 2018; 51: 55–61. https://doi.org/10.1016/j.ppedcard.2018.10.004
3. Ramlawi B, Reardon MJ. Cardiac Tumors: Treatment. Clinical Cardio-oncology. Elsevier; 2016. https://doi.org/10.1016/B978-0-323-44227-5.00006–5
4. Singh GK, Mowers KL, Marino C, Balzer D, Rao PS. Effect of Pressure Recovery on Pressure Gradients in Congenital Stenotic Outflow Lesions in Pediatric Patients—Clinical Implications of Lesion

Severity and Geometry: A Simultaneous Doppler Echocardiography and Cardiac Catheter Correlative Study. J Am Soc Echocardiogr. 2020; 33: 207–217. https://doi.org/10.1016/j.echo.2019.09.001 PMID: 31699474

5. Feltes TF, Bacha E, Beekman RH, Cheatham JP, Feinstein JA, Gomes AS, et al. Indications for cardiac catheterization and intervention in pediatric cardiac disease: A scientific statement from the American Heart Association. Circulation. 2011; 123: 2607–2652. https://doi.org/10.1161/CIR.0b013e31821b1f10 PMID: 21536996
6. Villavicencio RE, Forbes TJ, Thomas RL, Humes RA. Pressure recovery in pediatric aortic valve stenosis. Pediatr Cardiol. 2003; 24: 457–462. https://doi.org/10.1007/s00246-002-0361-7 PMID: 14627313
7. Susin FM. Complete Unsteady One-Dimensional Model of the Net Aortic Pressure Drop. Open Biomed Eng J. 2019; 13: 83–93. https://doi.org/10.2174/1874120701913010083
8. Keshavarz-Motamed Z, Motamed PK, Maftoon N. Non-invasive determination of transcatheter pressure gradient in stenotic aortic valves: An analytical model. Med Eng Phys. 2015; 37: 321–327. https://doi.org/10.1016/j.medengphy.2015.01.003 PMID: 25682932
9. Garcia D, Pibarot P, Durand LG. Analytical modeling of the instantaneous pressure gradient across the aortic valve. J Biomech. 2005; 38: 1303–1311. https://doi.org/10.1016/j.jbiomech.2004.06.018 PMID: 15863115
10. Bermejo J, Antoranz JC, Burwash IG, Alvarez JLR, Moreno M, García-Fernández MA, et al. In-vivo analysis of the instantaneous transvalvular pressure difference-flow relationship in aortic valve stenosis: implications of unsteady fluid-dynamics for the clinical assessment of disease severity. J Heart Valve Dis. 2002; 11: 557–66. Available: http://www.ncbi.nlm.nih.gov/pubmed/12150306 PMID: 12150306
11. Fiore GB, Grigioni M, Daniele C, D'Avenio G, Barbaro V, Fumero R. Hydraulic functional characterisation of aortic mechanical heart valve prostheses through lumped-parameter modelling. J Biomech. 2002; 35: 1427–1432. https://doi.org/10.1016/s0021-9290(02)00177-x PMID: 12231289
12. Aboelkassem Y, Savic D, Campbell SG. Mathematical modeling of aortic valve dynamics during systole. J Theor Biol. 2015; 365: 280–288. https://doi.org/10.1016/j.jtbi.2014.10.027 PMID: 25451522
13. Padalino MA, Basso C, Moreolo GS, Thiene G, Stellin G. Left atrial myxoma in a child: Case report and review of the literature. Cardiovasc Pathol. 2003; 12: 233–236. https://doi.org/10.1016/s1054-8807(03)00037-1 PMID: 12826294
14. Garcia D, Pibarot P, Dumesnil JG, Sakr F, Durand LG. Assessment of aortic valve stenosis severity: A new index based on the energy loss concept. Circulation. 2000; 101: 765–771. https://doi.org/10.1161/01.cir.101.7.765 PMID: 10683350
15. Murphy DJ, Ge Y, Don CW, Keraliya A, Aghayev A, Morgan R, et al. Use of cardiac computerized tomography to predict neo-left ventricular outflow tract obstruction before transcatheter mitral valve replacement. J Am Heart Assoc. 2017; 6: 1–13. https://doi.org/10.1161/JAHA.117.007353 PMID: 29102981
16. White FM. Fluid mechanics. Seventh Ed. Mcgraw-Hill series in mechanical engineering; 2011.
17. Comunale G, Susin FM, Mynard JP. A female-specific cardiovascular lumped-parameter model. 2020 42nd Annual International Conference of the IEEE Engineering in Medicine & Biology Society (EMBC). Montréal, Québec, Canada: IEEE; 2020. pp. 2654–2657. https://doi.org/10.1109/EMBC44109.2020.9175427
18. Boville B, Young LC. Quick Guide to Pediatric Cardiopulmonary Care. Irvine, CA: EdwardsCritical Care Education; 2015. https://doi.org/10.1097/PCC.0000000000000338 PMID: 25607739
19. Chavhan GB, Parra DA, Mann A, Navarro OM. Normal doppler spectral waveforms of major pediatric vessels: Specific patterns. Radiographics. 2008; 28: 691–706. https://doi.org/10.1148/rg.283075095 PMID: 18480479
20. Murakami T, Takeda A, Takei K, Tateno S, Kawasoe Y, Niwa K. The cardiac blood supply–workload balance in children. Heart Vessels. 2015; 30: 626–631. https://doi.org/10.1007/s00380-014-0537-0 PMID: 24989969
21. Hegde S V., Lensing SY, Greenberg SB. Determining the normal aorta size in children. Radiology. 2015; 274: 859–865. https://doi.org/10.1148/radiol.14140500 PMID: 25469783
22. Gómez de Diego JJ, Gimelli A, Chubuchny V, Emilio P. Quantification of severity. In: EACVI Valvular Imaging Box [Internet]. Available: https://www.escardio.org/Education/Practice-Tools/EACVI-toolboxes/Valvular-Imaging/Atlas-of-valvular-imaging/4-2-Quantification-of-severity
23. Saouti N, Westerhof N, Postmus PE, Vonk-Noordegraaf A. The arterial load in pulmonary hypertension. Eur Respir Rev. 2010; 19: 197–203. https://doi.org/10.1183/09059180.00002210 PMID: 20956192
24. De Vecchi A, Marlevi D, Nordsletten DA, Ntalas I, Leipsic J, Bapat V, et al. Left ventricular outflow obstruction predicts increase in systolic pressure gradients and blood residence time after transcatheter

mitral valve replacement. Sci Rep. 2018; 8: 1–11. https://doi.org/10.1038/s41598-017-17765-5 PMID: 29311619

25. Butera G, Chessa M, Eicken A, Thomson J. Cardiac catheterization for congenital heart disease: From fetal life to adulthood. Card Catheter Congenit Hear Dis From Fetal Life to Adulthood. 2015; 1–786. https://doi.org/10.1007/978-88-470-5681-7

26. Keshavarz-Motamed Z. A diagnostic, monitoring, and predictive tool for patients with complex valvular, vascular and ventricular diseases. Sci Rep. 2020; 10: 1–19. https://doi.org/10.1038/s41598-020-63728-8 PMID: 32327673

27. Keshavarz-Motamed Z, Garcia J, Pibarot P, Larose E, Kadem L. Modeling the impact of concomitant aortic stenosis and coarctation of the aorta on left ventricular workload. J Biomech. 2011; 44: 2817–2825. https://doi.org/10.1016/j.jbiomech.2011.08.001 PMID: 21955730

28. Rajani R, Hancock J, Chambers JB. The art of assessing aortic stenosis. Heart. 2012; 98. https://doi.org/10.1136/heartjnl-2012-302392 PMID: 23143121

29. Zoghbi WA, Chambers JB, Dumesnil JG, Foster E, Gottdiener JS, Grayburn PA, et al. Recommendations for Evaluation of Prosthetic Valves With Echocardiography and Doppler Ultrasound. A Report From the American Society of Echocardiography's Guidelines and Standards Committee and the Task Force on Prosthetic Valves, Developed in Conjunction. J Am Soc Echocardiogr. 2009; 22: 975–1014. https://doi.org/10.1016/j.echo.2009.07.013 PMID: 19733789

30. Baumgartner H, Hung J, Bermejo J, Chambers JB, Evangelista A, Griffin BP, et al. Echocardiographic Assessment of Valve Stenosis: EAE/ASE Recommendations for Clinical Practice. J Am Soc Echocardiogr. 2009; 22: 1–23. https://doi.org/10.1016/j.echo.2008.11.029 PMID: 19130998

31. Krishna MR, Marathe SP, Maghsoudi A, McCowage G, Sherwood MC, Orr Y. Emergency Ross Procedure for Pediatric Aortic Valve Myxofibrosarcoma. Ann Thorac Surg. 2019; 107: e183–e185. https://doi.org/10.1016/j.athoracsur.2018.07.060 PMID: 30266618

32. Delmo Walter EM, Javier MF, Sander F, Hartmann B, Ekkernkamp A, Hetzer R. Primary Cardiac Tumors in Infants and Children: Surgical Strategy and Long-Term Outcome. Ann Thorac Surg. 2016; 102: 2062–2069. https://doi.org/10.1016/j.athoracsur.2016.04.057 PMID: 27344282

33. Padalino MA, Vida VL, Boccuzzo G, Tonello M, Sarris GE, Berggren H, et al. Surgery for primary cardiac tumors in children early and late results in a multicenter european congenital heart surgeons association study. Circulation. 2012; 126: 22–30. https://doi.org/10.1161/CIRCULATIONAHA.111.037226 PMID: 22626745

34. Foschi M, Di Mauro M, Tancredi F, Capparuccia C, Petroni R, Leonzio L, et al. The Dark Side of the Moon: The Right Ventricle. J Cardiovasc Dev Dis. 2017; 4: 18. https://doi.org/10.3390/jcdd4040018 PMID: 29367547

35. Haddad F, Doyle R, Murphy DJ, Hunt SA. Right ventricular function in cardiovascular disease, part II: Pathophysiology, clinical importance, and management of right ventricular failure. Circulation. 2008; 117: 1717–1731. https://doi.org/10.1161/CIRCULATIONAHA.107.653584 PMID: 18378625

36. Ventetuolo CE, Klinger JR. Management of acute right ventricular failure in the intensive care unit. Ann Am Thorac Soc. 2014; 11: 811–822. https://doi.org/10.1513/AnnalsATS.201312-446FR PMID: 24828526

37. Bonow RO, Carabello BA, Chatterjee K, de Leon AC, Faxon DP, Freed MD, et al. 2008 Focused Update Incorporated Into the ACC/AHA 2006 Guidelines for the Management of Patients With Valvular Heart Disease. A Report of the American College of Cardiology/American Heart Association Task Force on Practice Guidelines (Writing Committee to. J Am Coll Cardiol. 2008;52. https://doi.org/10.1016/j.jacc.2008.03.034 PMID: 18582635

38. Garcia J, Kadem L, Larose E, Clavel MA, Pibarot P. Comparison between cardiovascular magnetic resonance and transthoracic doppler echocardiography for the estimation of effective orifice area in aortic stenosis. J Cardiovasc Magn Reson. 2011; 13: 25. https://doi.org/10.1186/1532-429X-13-25 PMID: 21527021

39. Izumo M, Shiota M, Saitoh T, Kuwahara E, Fukuoka Y, Gurudevan S V., et al. Non-circular shape of right ventricular outflow tract a real-time 3-dimensional transesophageal echocardiography study. Circ Cardiovasc Imaging. 2012; 5: 621–627. https://doi.org/10.1161/CIRCIMAGING.112.974287 PMID: 22891043

40. Koto D, Izumo M, Machida T, Suzuki K, Yoneyama K, Suzuki T, et al. Geometry of the left ventricular outflow tract assessed by 3D TEE in patients with aortic stenosis: impact of upper septal hypertrophy on measurements of Doppler-derived left ventricular stroke volume. J Echocardiogr. 2018; 16: 162–172. https://doi.org/10.1007/s12574-018-0383-7 PMID: 29797230

41. Hagendorff A, Knebel F, Helfen A, Knierim J, Sinning C, Stöbe S, et al. Expert consensus document on the assessment of the severity of aortic valve stenosis by echocardiography to provide diagnostic

conclusiveness by standardized verifiable documentation. Clin Res Cardiol. 2020; 109: 271–288. https://doi.org/10.1007/s00392-019-01539-2 PMID: 31482241

42. Singh GK. Congenital Aortic Valve Stenosis. Children. 2019; 6: 1–13. https://doi.org/10.3390/children6050069 PMID: 31086112